Front. Earth Sci. 2018, 12(1): 1–16
https://doi.org/10.1007/s11707-017-0671-y

RESEARCH ARTICLE

Effects of diurnal adjustment on biases and trends derived from inter-sensor calibrated AMSU-A data

H. CHEN[1], X. ZOU (✉)[2], Z. QIN[3]

1 Department of Atmospheric and Oceanic Sciences, University of Colorado, Boulder, Colorado, CO 80309, USA
2 Earth System Science Interdisciplinary Center (ESSIC), University of Maryland, College Park, Maryland, MD 20742, USA
3 Joint Center for Data Assimilation Research and Applications, Nanjing University of Information Science and Technology, Nanjing 210044, China

Abstract Measurements of brightness temperatures from Advanced Microwave Sounding Unit-A (AMSU-A) temperature sounding instruments onboard NOAA Polar-orbiting Operational Environmental Satellites (POES) have been extensively used for studying atmospheric temperature trends over the past several decades. Inter-sensor biases, orbital drifts and diurnal variations of atmospheric and surface temperatures must be considered before using a merged long-term time series of AMSU-A measurements from NOAA-15, -18, -19 and MetOp-A. We study the impacts of the orbital drift and orbital differences of local equator crossing times (LECTs) on temperature trends derivable from AMSU-A using near-nadir observations from NOAA-15, NOAA-18, NOAA-19, and MetOp-A during 1998 – 2014 over the Amazon rainforest. The double difference method is firstly applied to estimation of inter-sensor biases between any two satellites during their overlapping time period. The inter-calibrated observations are then used to generate a monthly mean diurnal cycle of brightness temperature for each AMSU-A channel. A diurnal correction is finally applied each channel to obtain AMSU-A data valid at the same local time. Impacts of the inter-sensor bias correction and diurnal correction on the AMSU-A derived long-term atmospheric temperature trends are separately quantified and compared with those derived from original data. It is shown that the orbital drift and differences of LECT among different POESs induce a large uncertainty in AMSU-A derived long-term warming/cooling trends. After applying an inter-sensor bias correction and a diurnal correction, the warming trends at different local times, which are approximately the same, are smaller by half than the trends derived without applying these corrections.

Received April 29, 2017; accepted July 16, 2017

E-mail: xzou1@umd.edu

Keywords AMSU-A, diurnal adjustment, decadal temperature trend

1 Introduction

The Advanced Microwave Sounding Unit-A (AMSU-A) is a cross-track temperature sounding radiometer. It came into use since the launch of National Oceanic and Atmospheric Administration (NOAA)-15 on 13 May 1998. NOAA-16, -17, -18, and -19 all carried AMSU-A when they were successively launched during the time period from 1998 to 2009. The AMSU-A has also been flying on the National Aeronautics and Space Administration (NASA) Aqua Earth science satellite and the European Organization for the Exploitation of Meteorological Satellites (EUMETSAT) Meteorological Operational (MetOp) series MetOp-A, -B. The AMSU-A provides 12 temperature-sounding channels that are located in the oxygen absorption band within the microwave spectral range from 50.3 to 57.3 GHz for profiling atmospheric temperatures in the troposphere and low stratosphere (Mo, 1996), as well as three additional window channels to provide simultaneously information of water vapor, cloud, and precipitation within atmospheric columns (Weng and Grody, 2000).

The AMSU-A observations are invaluable not only to numerical weather prediction (NWP) (Andersson et al., 1991; Eyre et al., 1993; Derber and Wu, 1998), but also to climate studies (Zou et al., 2006, 2011; Zou and Wang, 2011; Wang et al., 2011). However, Polar-orbiting Operational Environmental Satellites (POES) satellites have limited life spans. Before AMSU-A data from different satellites are merged together for climate applications, an inter-calibration among different POES AMSU-A instruments must be carried out (Zou and Wang, 2011). A simultaneous nadir overpass (SNO) method that is based

on finding cross-over points near the Polar Regions between two instruments (Cao et al., 2004) could be used for the inter-calibration for microwave radiometers on board Polar Operational Environmental Satellites (POES) (Zou et al., 2006, 2014). Due to a limitation of the SNO method producing a too small sampling size, an inter-calibration algorithm based on the Double Difference (DD) method was developed to explain the geophysical variability of the brightness temperature measurements from different instruments, as well as the individual instrument characteristics such as center frequency, earth incidence angle etc. (Kroodsma et al., 2012). It was shown that the DD method provided consistent results with SNO methods for when the same amount of data samples were used (Wang et al., 2011). The DD method is adopted for this study to conduct an inter-sensor bias correction.

In addition to an inter-sensor bias correction, a diurnal correction is required for climate study based on the long-term time series of AMSU-A data from different POES. Ideally, a sun-synchronous satellite orbits around the Earth and passes over the equator at two fixed local equator crossing times (LECTs). A complete orbit around the Earth takes about 103 minutes. In other words, an AMSU-A instrument onboard POES takes measurements over a targeted geographical location twice daily at two fixed local times that are different from LECT for no more than 52 minutes on its ascending and descending nodes. However, in practice, the satellite could drift slowly away from its previous orbit due to atmospheric drag, inhomogeneous gravitational fields of the Earth and other factors (Privette et al., 1995). If a POES orbit experiences such a drift, the LECT would change. Averaging the ascending and descending orbital observations would not completely cancel out the diurnal signals since the diurnal cycle has an asymmetric feature. A diurnal correction must be implemented before deriving global warming or cooling trends from AMSU-A data. Mears et al. (2002) employed a climate-model based method for estimating the diurnal-cycle variation of brightness temperature on a 128x64 grid of Earth locations for carrying out diurnal correction. Specifically, the National Center for Atmospheric Research NCAR Community Climate Model (CCM3) was employed to produce hourly global gridded data of atmospheric state variables such as atmospheric temperature and humidity profiles and surface temperatures. The model-produced global data were then used as inputs to a microwave radiative transfer model in order to simulate the brightness temperatures for Microwave Sounding Unit (MSU). The diurnal-cycle variation at each grid point was finally estimated from the hourly datasets of MSU brightness temperature simulations.

It is pointed out that the accuracy of the simulated diurnal cycles would naturally depend on both the CCM3 forecasts and the radiative transfer model. Model errors on diurnal cycles would then affect the trends derived from the satellite data. In this study, AMSU-A data from NOAA-15, -18, -19 and MetOp-A are chosen for use directly to derive temperature trends by carrying out firstly an inter-calibration and secondly a diurnal correction. The paper is organized as follows: Section 2 gives a brief description of the double difference method and diurnal correction method. The results for inter-sensor biases and diurnal-cycle variations are provided in sections 3 and 4. Impacts of diurnal corrections on trends are provided in section 5. Summary and conclusions are given in section 6.

2 Methods and methodology

2.1 AMSU-A data

AMSU-A is a cross-track instrument that measures globally atmospheric and surface radiations in the microwave spectra at 23.8 GHz (channel 1), 31. 4 GHz (channel 2) and 89 GHz (channel 15), as well as between 50.3 GHz (channel 3) and $57.29\pm 0.322\pm 0.0045$ GHz (channel 14). Channels 1, 2, and 15 are window channels with their peak weighting functions located at the surface. Channels 3 – 14 are temperature-sounding channels with their peak weighting functions located around (950, 850, 700, 400, 250, 200, 100, 50, 25, 10, and 5) hPa (Tian and Zou, 2016). There are a total of 30 Field Of Views (FOVs) per scan, and the swath width is about 2300 km. The largest scan angles of AMSU-A from nadir are $\pm 48.3°$. The FOV positions 15 and 16 have a near-nadir angle of 1.67° and their nominal spatial resolution is about 48 km. A single scan cycle of AMSU-A takes 8 seconds.

The AMSU-A data chosen for this study are those from NOAA-15, -18, -19 and MetOp-A over the Amazon rainforest (1°S – 4°N, 53°W – 59°W), which is one of the largest homogeneous land areas on the Earth. The stability of AMSU-A data over this region is due to the dense canopy that heavily attenuates the surface radiation so that only emissions from the canopy and atmosphere contribute to the AMSU-A observation (Mo, 2007).

It is noted that data from channels 6, 11, and 14 of NOAA-15, channel 8 of NOAA-19, and channel 7 of MetOp-A are excluded from this study since these channels were out of use. Also, unphysical measurements (negative brightness temperatures) are removed from the time series of AMSU-A data.

2.2 Double difference method

The long-term brightness temperature observations from AMSU-A onboard NOAA-15, -18, -19 and MetOp-A were inter-calibrated using the DD method. The AMSU-A brightness temperature observations from NOAA-18 are used as the reference data for the DD method, i.e., AMSU-A data from NOAA-15, NOAA-19, and MetOp-A are paired with AMSU-A data from NOAA-18. The AMSU-A data within the specified overlapping time period of the

paired satellites (see Table 1) are used in the DD method. The AMSU-A data from each satellite pair are further divided into pentad (5-day) datasets for reducing impacts of data noise on biases derived from the DD method. Only the near-nadir observations (e.g., FOVs 15 and 16) over ocean under clear-sky conditions are selected. The clear-sky conditions are defined as LWP$\leqslant$0.01 kg·m^{-2}, where LWP is the cloud liquid water path derived from AMSU-A window channels 1 and 2. Details for the LWP retrieval algorithm can be found in Weng et al. (2003).

Table 1 The overlapping AMSU-A time periods for paired satellite datasets

Satellite Paired with NOAA-18	Start date	End date
NOAA-15	2005-05-24	2012-07-01
NOAA-19	2009-08-01	2013-03-28
MetOp-A	2007-05-24	2011-04-23

The Community Radiative Transfer Model (CRTM) developed by the US Joint Center for Satellite Data Assimilation (Han et al., 2007; Weng, 2007) is used for obtaining simulated brightness temperatures for all the selected AMSU-A observations. The inputs required by CRTM include sensor information such as zenith angles and locations, and model forecasts for surface parameters and temperature and humidity profiles. The global model forecast fields of the National Centers for Environmental Prediction (NCEP) final operational global analysis (FNL) data is used for the model simulations. By comparing with an accurate line-by-line radiative transfer model (RTM) — the Atmospheric and Environmental Research Inc. (AER) Monochromatic Radiation Transfer Model (MonoRTM) (Clough et al., 2005), Zou et al. (2011) showed that the CRTM simulations in clear-sky conditions are quite accurate.

For brevity, the AMSU-A observations are indicated as O, and the CRTM simulations are indicated as B. For a given channel,

$$\overline{O_{\rm sat}-B_{\rm sat}}=\overline{\mu_{O,\,\rm sat}}-\overline{\mu_{B,\,\rm sat}}, \quad (1)$$

$$\overline{O_{\rm NOAA-18}-B_{\rm NOAA-18}}=\overline{\mu_{O,\,\rm NOAA-18}}-\overline{\mu_{B,\,\rm NOAA-18}}, \quad (2)$$

where the subscript "sat" indicates the AMSU-A data from one of NOAA-15, NOAA-19, and MetOp-A, $\overline{\mu_{O,\,\rm sat}}=\overline{O_{\rm sat}-T_{\rm b,\,true}}$ represents the observation biases, $\overline{\mu_{B,\,\rm sat}}=\overline{B_{\rm sat}-T_{\rm b,\,true}}$ is the model biases.

Taking the differences of both sides between Eqs. (1) and (2) yields:

$$\overline{O_{\rm sat}-B_{\rm sat}}-\overline{O_{\rm NOAA-18}-B_{\rm NOAA-18}}=(\overline{\mu_{O,\,\rm sat}}-\overline{\mu_{O,\,\rm NOAA-18}})-(\overline{\mu_{B,\,\rm sat}}-\overline{\mu_{B,\,\rm NOAA-18}}). \quad (3)$$

Since the model and global forecasts used for simulations for different sensors are the same, and the systematic errors of both CRTM and NCEP FNL datasets are stable, the long-term mean of $\overline{\mu_B}$ is assumed to be the same for all the sensors, which lead to

$$(\overline{\mu_{B,\,\rm sat}}-\overline{\mu_{B,\,\rm NOAA-18}})=0. \quad (4)$$

Equation (3) can then be simplified as:

$$\overline{O_{\rm sat}-B_{\rm sat}}-\overline{O_{\rm NOAA-18}-B_{\rm NOAA-18}}=\overline{\mu_{O,\,\rm sat}}-\overline{\mu_{O,\,\rm NOAA-18}}, \quad (5)$$

where $\overline{\mu_{O,\,\rm sat}}-\overline{\mu_{O,\,\rm NOAA-18}}$ represents the inter-sensor bias between the satellite "sat" (e.g., NOAA-15, -19 or MetOp-A) and NOAA-18.

Based on Eq. (5), an inter-sensor bias can be obtained from each paired pentad dataset. We may write down a final expression for the inter-sensor bias between "sat" and NOAA-18 ($\mu_{DD,\,\rm sat}$) as follows:

$$\mu_{DD,\,\rm sat}=\overline{\overline{O_{\rm sat}-B_{\rm sat}}-\overline{O_{\rm NOAA-18}-B_{\rm NOAA-18}}}. \quad (6)$$

2.3 Mathematical formulation of the diurnal cycle

To implement the diurnal correction, the diurnal-cycle variations of brightness temperatures need to be firstly calculated for all AMSU-A channels included in this study. This study employs a method similar to Mo (2007) for calculating the diurnal-cycle variation of the brightness temperature for AMSU-A. For a given region, the diurnal cycles are calculated based on the monthly mean data for each channel of AMSU-A. For each channel, diurnal-cycle variations in all 12 months in a year are calculated.

In the following, the procedure for calculating diurnal variation is provided using AMSU-A channel 1 data in January over the Amazon rainforest as an example. Brightness temperature observations over Amazon rainforest in January under "no-rain" conditions are selected from AMSU-A onboard NOAA-15, -18, -19, and MetOp-A each year. The AMSU-A data in rainy conditions could be detected based on the depression of the high frequency channel 15. Following Ferraro et al. (2000), the scattering index ($SI_{89}=T_{\rm b,\,ch1}-T_{\rm b,\,ch15}$) being greater than 3 K detects rainfall. In other words, the "no-rain" condition is defined when the difference between the brightness temperature of channels 1 and 15 is less than or equal to 3.0 K ($SI_{89}\leqslant$3.0 K). The local observational time for each selected observation is firstly obtained by converting the recorded Coordinated Universal Time (UTC) based on the longitude of the observation. The selected observations from NOAA-15, NOAA-19, and MetOp-A are inter-calibrated with respect to NOAA-18 using the inter-sensor bias obtained in Section 2.2. Every year, the AMSU-A data from different POES generate two (ascending/descending)

monthly means of AMSU-A brightness temperatures at different local times, which are denoted as $\overline{T_{\mathrm{b,\,obs}}}(\bar{t})$, $\bar{t}$ is the monthly mean local time with the unit of hour. The values of $\overline{T_{\mathrm{b,\,obs}}}(\bar{t})$ are calculated from all available AMSU-A data on board NOAA-15, -18, -19, and MetOp-A.

After all the $\overline{T_{\mathrm{b,\,obs}}}(\bar{t})$ are obtained, the diurnal cycle is estimated using the second-order Fourier series expressed by the following equation:

$$T_{\mathrm{dc}} = A_0 + \sum_{n=1}^{2}(A_n \sin n\theta + B_n \cos n\theta)$$

$$= A_0 + A_1 \sin\theta + B_1 \cos\theta + A_2 \sin 2\theta + B_2 \cos 2\theta, \quad (7)$$

where $\theta = \frac{\pi \bar{t}}{12}$ and $0 \leqslant \bar{t} \leqslant 24$ h, and A_0, A_1, B_1, A_2, and B_2 are unknown coefficients to be found from the data $\overline{T_{\mathrm{b,\,obs}}}(\bar{t})$ during an overlapping time period of NOAA-15, -18, -19, and MetOp-A. $\overline{T_{\mathrm{b,\,obs}}}(\bar{t})$ can be expressed as $\overline{T_{\mathrm{b,\,obs}}}(\theta_k) k = 1, 2, ..., N$, where N is the total number of $\overline{T_{\mathrm{b,\,obs}}}(\theta)$. Coefficients A_0, A_1, B_1, A_2, and B_2 in Eq. (7) can be calculated from least square fitting method.

2.4 Linear trend calculation

The time series of AMSU-A brightness temperature observations are given as $\{(t_i, T_{\mathrm{b},\,i}), i = 1, 2, ..., n\}$, where t indicates the observational time with units of Julian day, and T_{b} indicates the brightness temperature observations. Assuming T_{b} varies linearly with t, which can be expressed as:

$$T_{\mathrm{b}} = \alpha + \beta t. \quad (8)$$

Then the coefficients of α and β are solved using least-square approach (Aldrich, 1998), i.e.,

$$\min_{\alpha,\,\beta}\left(\sum_{i=1}^{n}(T_{\mathrm{b},\,i} - \alpha - \beta t_i)^2\right). \quad (9)$$

The solutions for the coefficients of α and β are:

$$\beta^* = \frac{\sum_{i=1}^{n}(T_{\mathrm{b},\,i} - \overline{T_{\mathrm{b}}})(t_i - \bar{t})}{\sum_{i=1}^{n}(t_i - \bar{t})^2}, \quad (10a)$$

$$\alpha^* = \overline{T_{\mathrm{b}}} - \beta^* \bar{t}. \quad (10b)$$

3 Inter-sensor bias corrections

Time series of double difference results for channels 1 and 5 of AMSU-A from NOAA-15 and NOAA-18, NOAA-19 and NOAA-18, and MetOp-A and NOAA-18 are shown in Fig. 1. A colored single circle represents the double difference between NOAA-15 (or NOAA-19, MetOp-A) and NOAA-18 calculated using the double difference method described in Eq. (5). The mean values of all the colored circles are indicated by the solid lines with the same color convention as the individual results. The double difference results for each paired satellites at window channel 1 (Fig. 1(a)) have larger spreads than those of the sounding channel 5 (Fig. 1(b)). This is because window channel 1 is highly sensitive to the surface emissivity and thus has a larger variability and uncertainty than the temperature-sounding channel 5 located in the middle troposphere. It is also shown that the double difference results are stable with time. With NOAA-18 data as the reference, NOAA-15 and MetOp-A have positive constant mean inter-sensor biases of slightly different magnitudes while NOAA-19 has a negative mean inter-sensor bias.

In order to quantify and show the variability of the double difference results, a set of scatter plots of the double difference $\overline{(O-B)}_{\mathrm{sat}} - \overline{(O-B)}_{\mathrm{NOAA-18}}$ for AMSU-A channels 1 and 5 are provided in Fig. 2. The O and B are selected from pentad datasets under the condition of near-nadir (FOVs 15 and 16) and clear-sky over ocean within the latitudinal band of 1°S- 4°N during the overlapping period of two satellites (see Table 1). It is confirmed that the double differences for channel 1 have a larger spread than channel 5. A smaller standard deviation suggests a better representation of the inter-sensor bias.

The final values of the inter-sensor biases of all AMSU-A channels between NOAA-15 and NOAA-18, NOAA-19 and NOAA-18, and MetOp-A and NOAA-18 based on the estimation method described above are provided in Tables 2–4.

4 Diurnal-cycle variation over the Amazon rainforest

Variations of LECTs of NOAA-15, NOAA-18, NOAA-19, and MetOp-A from ascending and descending nodes over the Amazon rainforest during 1998 – 2014 are shown in Fig. 3. NOAA-15, NOAA-18, and NOAA-19 exhibit slow orbit drift. For NOAA-15, the ascending (descending) orbit drifted from a LECT around 2130 local time (LT) (0930 LT) in October 1998 to about 1640 LT (0440 LT) in June 2012. From May 2005 to March 2013, NOAA-18 drifted from 1400 LT to 1515 LT in LECTs. NOAA-19 drifted from 1350 LT to 1335 LT ECTs from August 2009 to March 2013. Since MetOp-A has an Attitude and Orbit Control Subsystem (AOCS) that can adjust the polar orbit during its lifespan, the LECTs of MetOp-A barely drifted. It is noted that as the orbit drifted, NOAA-15 changed from

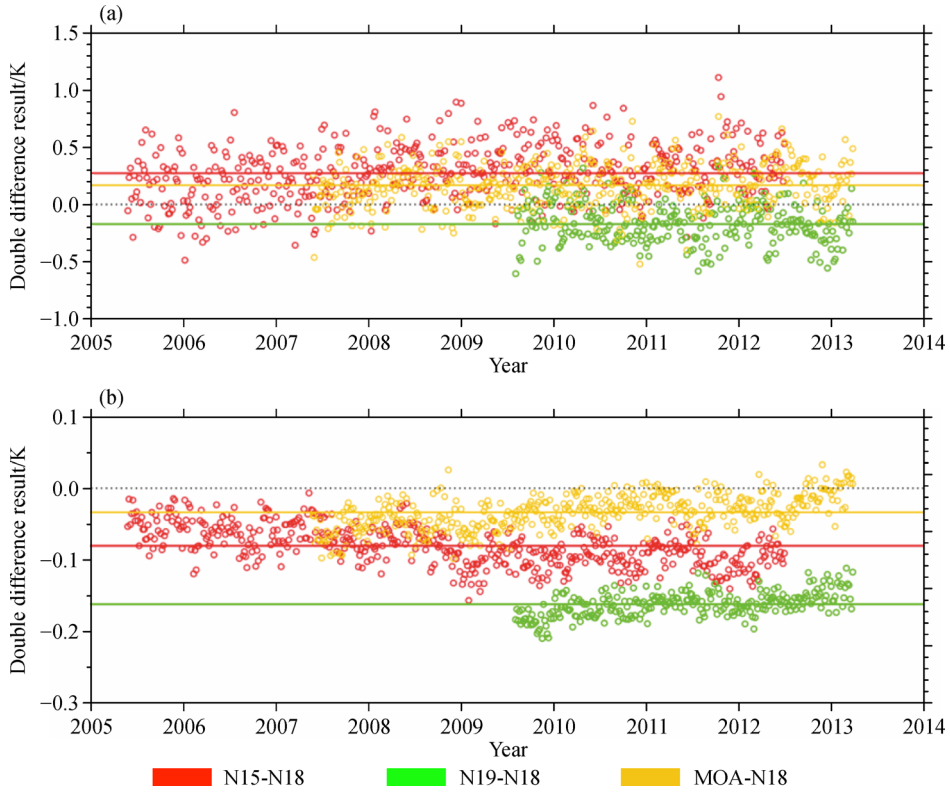

Fig. 1 Time series of double difference results for (a) channel 1 and (b) channel 5 of AMSU-A onboard NOAA-15 (N15), NOAA-19 (N19), MetOp-A (MOA) paired with AMSU-A onboard NOAA-18 (N18).

an early-morning satellite to an afternoon satellite during its long lifetime.

The brightness temperature observations of channel 1 at the descending and ascending nodes from NOAA-15, -18, -19, and MetOp-A on January 1st, 2012 are presented in Figs. 4(a) and 4(b), respectively. The brightness temperatures have a significant warming pattern increased as the LT changes from 0443 LT (NOAA-15 descending node) to 0949 LT (MetOp-A descending node) and decreased cooling pattern as the LT changes from 1504 LT (NOAA-18 ascending node) to 2114 LT (MetOp-A ascending node). Such warming and cooling patterns indicate the impact of a noticeably significant diurnal variation of AMSU-A brightness temperatures for channel 1 over the Amazon rainforest. Although the four satellites are all in the sun-synchronous orbits and able to provide global coverage of observations, the observation gaps occur when the ascending and descending orbits are studied separately, which are shown in blank area in Fig. 4(b).

The diurnal variations of brightness temperatures from all 15 AMSU-A channels in January, and results for channels 1, 5, 8, and 10 are shown in Fig. 5. The colored circles are the near-nadir observations under "no-rain" condition ($T_{b,ch1} - T_{b,ch15} \leqslant 3$ K). The mean values of the monthly observations, which are indicated by triangles in Fig. 5, are used to calculate the diurnal-cycle variation using the method described in Section 2.3. As mentioned before, the observations have been inter-calibrated with respected to observations from NOAA-18 to improve the consistency of the data from different satellites. Satellites that experience orbital drifts provide measurements at different local times. For example, when NOAA-15 drifted during the period from 1998 to 2012, this satellite provides measurements at the local times of 2130 LT and 0930 LT in 1998, but at 1640 LT and 0440 LT in 2012. The AMSU-A window channels 1, 2 and 15 have larger diurnal variations than the other 12 channels (results for only channel 1 is shown). Channel 8 shows a relatively small diurnal variation that the derived diurnal-cycle almost a horizontal straight line. The diurnal variations of channels 1, 2, 3, 4, 5, 7, and 15 show sinusoidal patterns with their maxima locating around the local time afternoon and minima in the local time morning (results for channels 1 and 5 are shown). However, for channels 6, 9, 10, 11, 12, and 14, the diurnal-cycle variations exhibit noticeable semi-diurnal signal with more than one maxima and minima. Further investigations are needed to find out reasons for these upper-level temperature-sounding channels to have not only diurnal but also semi-diurnal variations.

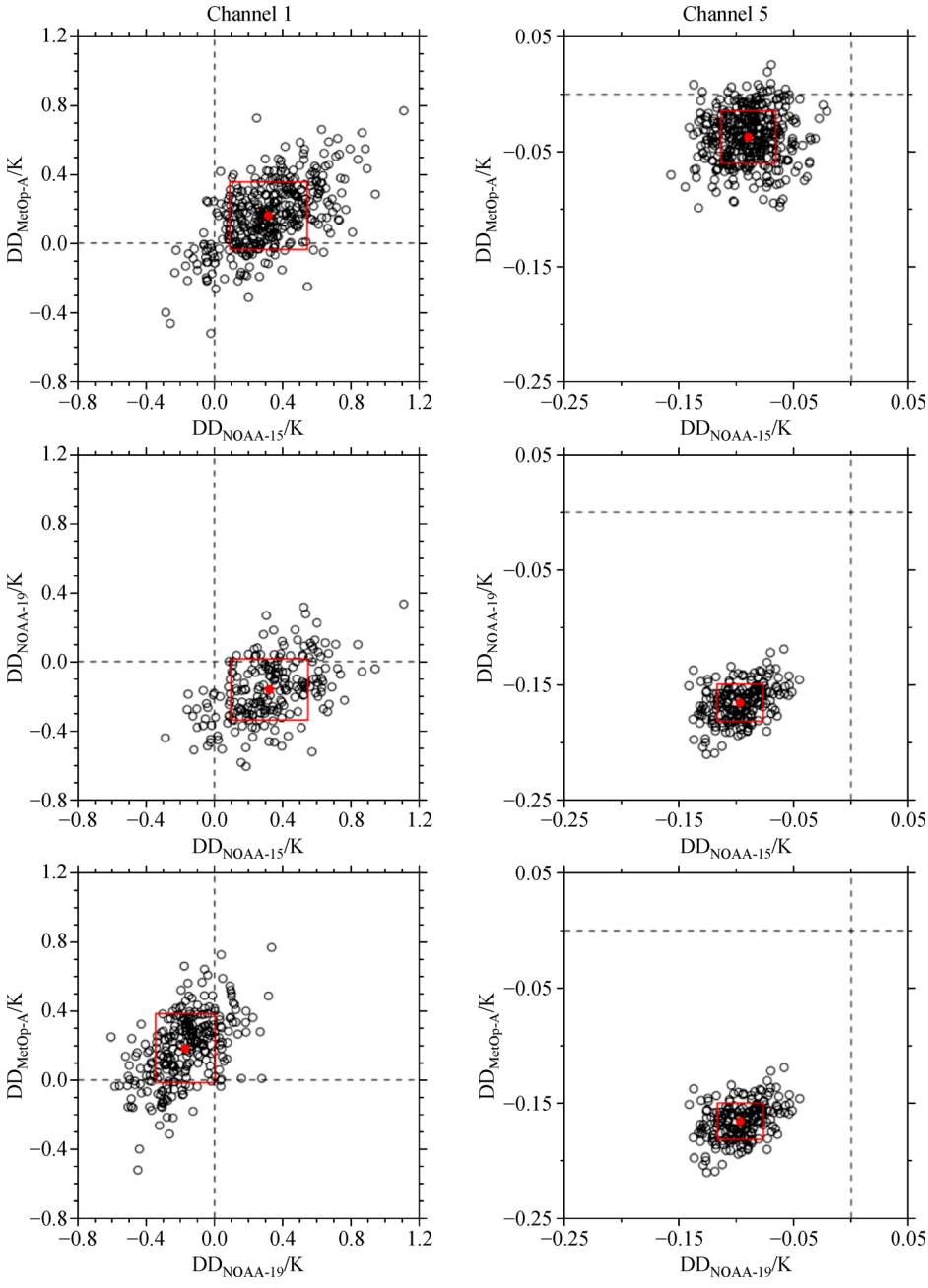

Fig. 2 Scatter plots of double differences $\overline{(O-B)}_{\mathrm{sat}}-\overline{(O-B)}_{\mathrm{NOAA-18}}$ for AMSU-A channels 1 (left panels) and 5 (right panels). The inter-sensor bias $\mu_{DD,\,\mathrm{sat}}$ and one-standard deviation are indicated by red dot and red box, respectively.

Table 2 The inter-sensor biases for AMSU-A channels 1- 15 (except for channels 6, 11, 14) between NOAA-15 and NOAA-18. The inter-sensor biases between sat and NOAA-18 are estimated by $\mu_{sat} = \overline{\overline{(O-B)}_{sat} - \overline{(O-B)}_{NOAA-18}}$. σ_{sat} is the standard deviation

Channel	μ_{sat}/K	σ_{sat}/K
1	0.272	0.241
2	0.085	0.162
3	−0.001	0.145
4	−0.121	0.047
5	−0.081	0.027
6	N/A	N/A
7	0.545	0.037
8	0.232	0.048
9	0.736	0.044
10	0.499	0.056
11	N/A	N/A
12	0.408	0.128
13	0.204	0.215
14	N/A	N/A
15	0.303	0.257

Table 3 Same as Table 2 except for NOAA-19 and NOAA-18

Channel	μ_{sat}/K	σ_{sat}/K
1	−0.172	0.175
2	−0.231	0.112
3	−0.105	0.121
4	−0.016	0.028
5	−0.162	0.017
6	0.231	0.017
7	0.437	0.041
8	N/A	N/A
9	0.485	0.037
10	0.463	0.039
11	0.502	0.056
12	0.381	0.095
13	0.594	0.147
14	0.218	0.173
15	0.319	0.179

5 Impacts of diurnal corrections on trends

For a given region, the diurnal correction is a method to map the brightness temperature (T_b^{obs}) measured at different local times to a same reference local time based on the calculated diurnal-cycle variation of T_{dc}. The diurnal correction can be described as the following equation (Mears et al., 2002):

Table 4 Same as Table 3 except for MetOp-A and NOAA-18

Channel	μ_{sat}/K	σ_{sat}/K
1	0.165	0.194
2	0.069	0.127
3	−0.041	0.122
4	0.041	0.034
5	−0.034	0.024
6	0.162	0.027
7	N/A	N/A
8	0.205	0.031
9	0.442	0.043
10	0.485	0.050
11	0.459	0.076
12	0.123	0.144
13	−0.651	0.241
14	−0.786	0.329
15	0.367	0.184

$$T_b^{corr}(t_{ref}) = T_b^{obs}(t_{obs}) + (T_{dc}(t_{ref}) - T_{dc}(t_{obs})), \quad (11)$$

where T_b^{obs} is the observed earth-scene brightness temperature, $T_{dc}(t)$ is the diurnal-cycle variation of brightness temperature at the local time t calculated by Eq. (7), t_{obs} is the local time of the observation, t_{ref} represents a selected reference time, and T_b^{corr} is the brightness temperature obtained after applying a diurnal correction.

Figure 6 shows the time series of brightness temperature observations of channel 1 from NOAA-15 from October 1998 to June 2012 before (Fig. 6(a)) and after (Fig. 6(b)) diurnal correction. The linear trend for the time series is indicated by the black solid line. It is reminded that only near-nadir observations under "no-rain" conditions over the Amazon rainforest are included in Fig. 6. The AMSU-A data from ascending and descending nodes are indicated in blue and red, respectively. Without a diurnal correction, the observations from the ascending nodes and the descending nodes gradually deviate apart from each other with time (Fig. 6(a)). The ascending data shows a warming trend while the descending data shows a slight cooling trend. The data from the ascending node also exhibit larger seasonal variations than the data from the descending nodes. After applying the diurnal correction, the data from different nodes achieved a high consistency and the annual variations are clearly seen in both the ascending and decending nodes (Fig. 6(b)). The warming trends are 0.909 K/decade and 0.398 K/decade without and with applying diurnal correction, respectively.

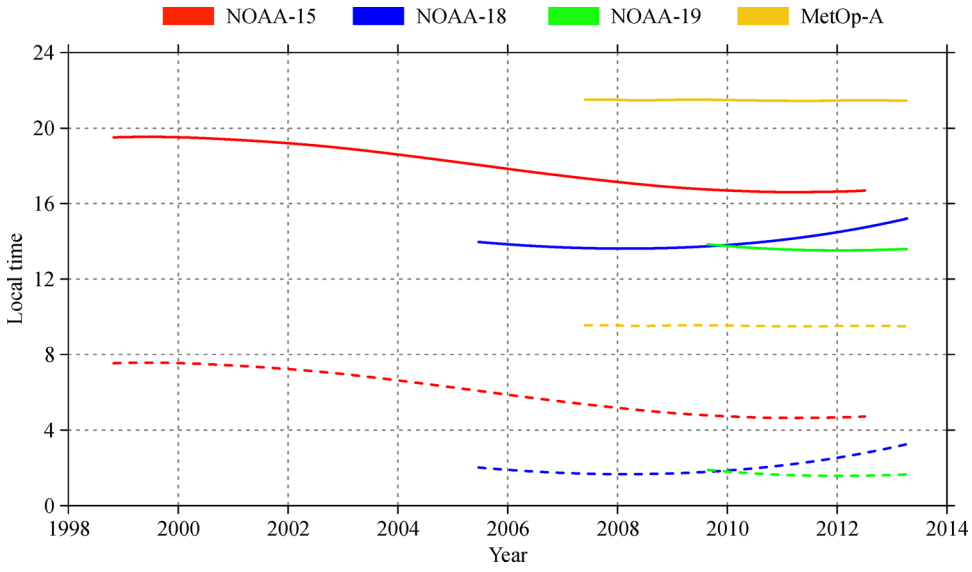

Fig. 3 Monthly mean of observational local times of multiple AMSU-As near-nadir observations from ascending nodes (solid lines) and descending nodes (dashed lines) over Amazon rainforest during 1998−2014.

Figure 7 is the same as Fig. 6 except for NOAA-15 channel 5. The data from the two different nodes of channel 5 also show better consistency after applying diurnal correction. The decadal trends for brightness temperatures of channel 5 from NOAA-15 without and with diurnal correction are 0.255 K/decade and 0.122 K/decade, respectively. It is noticed that the magnitude of correction for the ascending nodes is greater than that for descending nodes. This is because the NOAA-15 orbital drift brings stronger diurnal signals into the AMSU-A data at its ascending node, whose LECT changed from a nighttime 2130 LT to a late afternoon time 1640 LT during the period from October 1998 to June 2012. As the local time of ascending nodes changes from nighttime to afternoon, the brightness temperature increased as expected. The LECT change of the NOAA-15 ascending orbit gradually bought a warming signal from diurnal variation into the climate trend. On the other hand, the LECT of the NOAA-15 descending node changed from a morning time 0930 LT to an early morning time 0440 LT. The change of brightness temperature during morning is not as significant as that for the ascending nodes. The drift of descending orbit only brings a weak cooling diurnal signal into the AMSU-A data. This explains that the diurnal correction has larger impacts on the ascending than descending data and averaging the ascending and descending nodes would not cancel out the impact of diurnal variation due to a significant orbital drift.

Figure 8 shows the time series of NOAA-15 monthly mean brightness temperatures at channel 1 before and after applying diurnal correction at different reference local times. The monthly data counts are indicated by grey background. There was a noticeable seasonal variation of data count, which is associated with a seasonal variation of precipitation over the Amazon rainforest (Fig. 9). Since the symmetric diurnal-cycle signal is removed from the monthly mean data for which the ascending and descending nodes are averaged, the patterns of monthly means with and without applying diurnal correction result in small differences as expected.

The linear trends of brightness temperatures derived from monthly mean of NOAA-15 AMSU-A channel 1 before and after applying diurnal correction with different reference local times are shown in Fig. 10. The observations after applying diurnal correction at 0600, 0900, and 1200 LT have much smaller warming trends (colored lines) than that without the diurnal correction (black line). The trends for the diurnally corrected observations with different reference local times show relatively small differences. This implies that the choice of a reference local time has very little impact on the long-term trends, which is consistent with Mears et al. (2002).

Figure 11 presents the time series of channel 1 observations from NOAA-19, NOAA-18, NOAA-15, and MetOp-A with no inter-sensor bias correction nor diurnal correction (Fig. 11(a)), with inter-sensor bias correction only (Fig. 11(b)), and with both the inter-sensor bias correction and diurnal correction (Fig. 11(c)). Except for the morning satellite MetOp-A, observations from three afternoon NOAA satellites show large spreads (Fig. 11(a) and 11(b)), which are associated with the large differences between the brightness temperatures measured from the ascending nodes and descending nodes. This large spread disappeared significantly only after diurnal correction, and

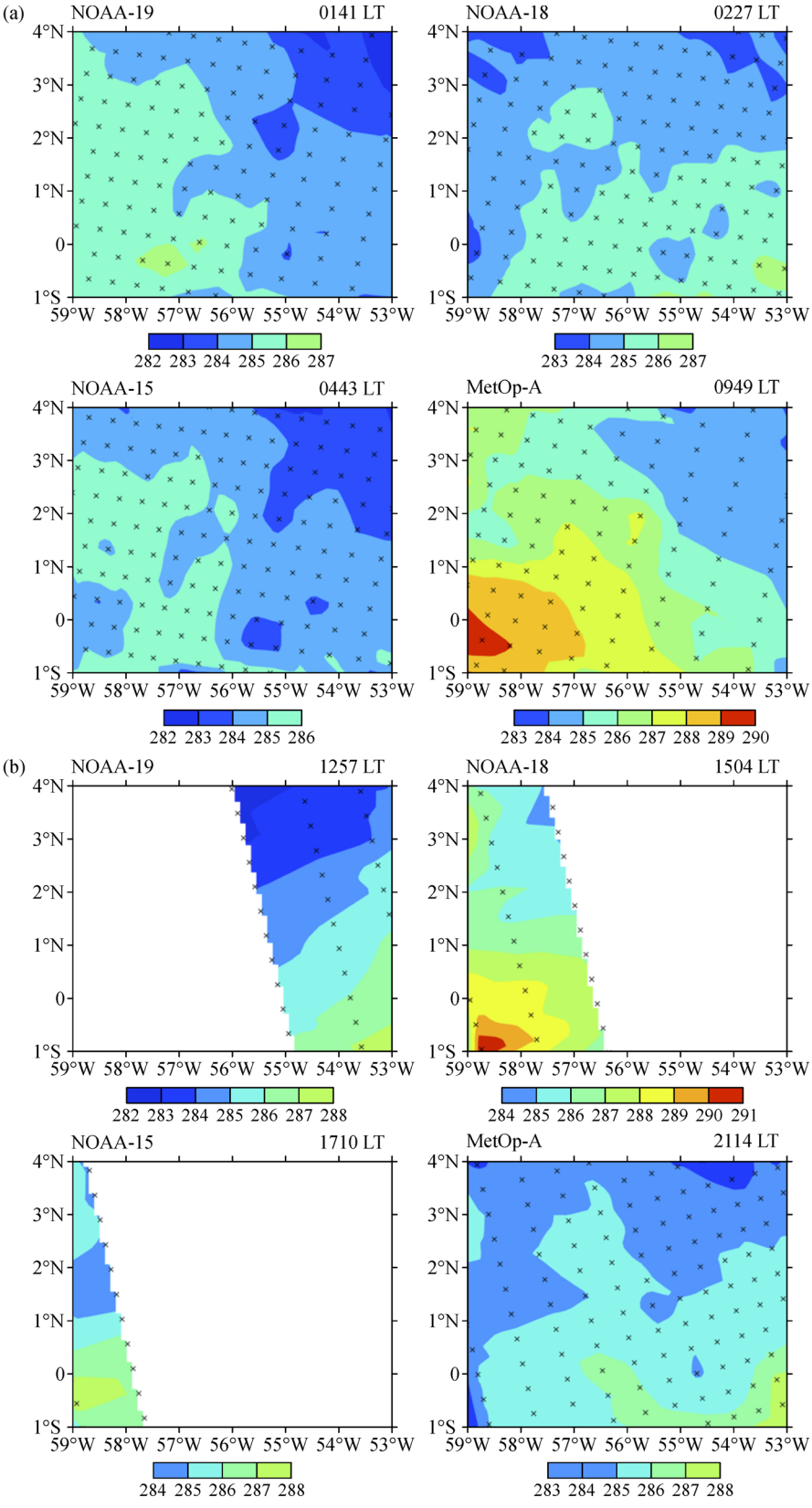

Fig. 4 Brightness temperature observations from AMSU-A channel 1 on (a) the descending nodes of NOAA-19, NOAA-18, NOAA-15 and MetOp-A which passed over Amazon rainforest around 0141 LT, 0227 LT, 0443 LT and 0949 LT January 1, 2012. AMSU-A FOV center locations are shown in black crosses; (b) the ascending nodes of NOAA-19, NOAA-18, NOAA-15 and MetOp-A over the Amazon rainforest around 1257 LT, 1504 LT, 1710 LT and 2114 LT.

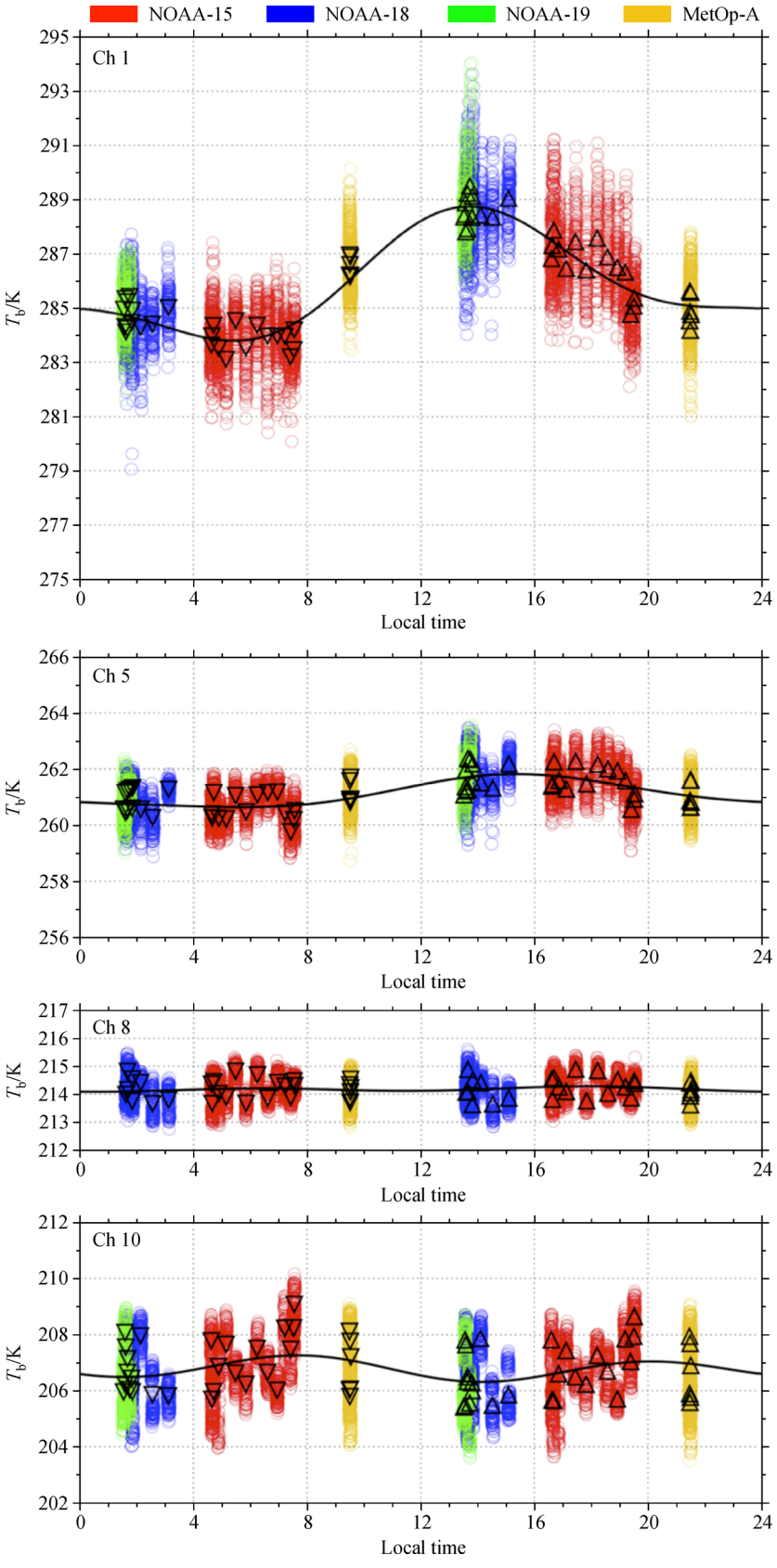

Fig. 5 Brightness temperature observations at FOVs 15 and 16 of channels 1, 5, 8 and 10 from NOAA-19, NOAA-18, NOAA-15 and MetOp-A under the "no-rain" conditions over Amazon rainforest in January (open circles) from 1999 to 2013. The monthly mean of near-nadir observations from descending nodes (down triangle) and ascending nodes (up triangle) are used for estimating the Fourier coefficients of the diurnal variation of brightness temperatures (black curve).

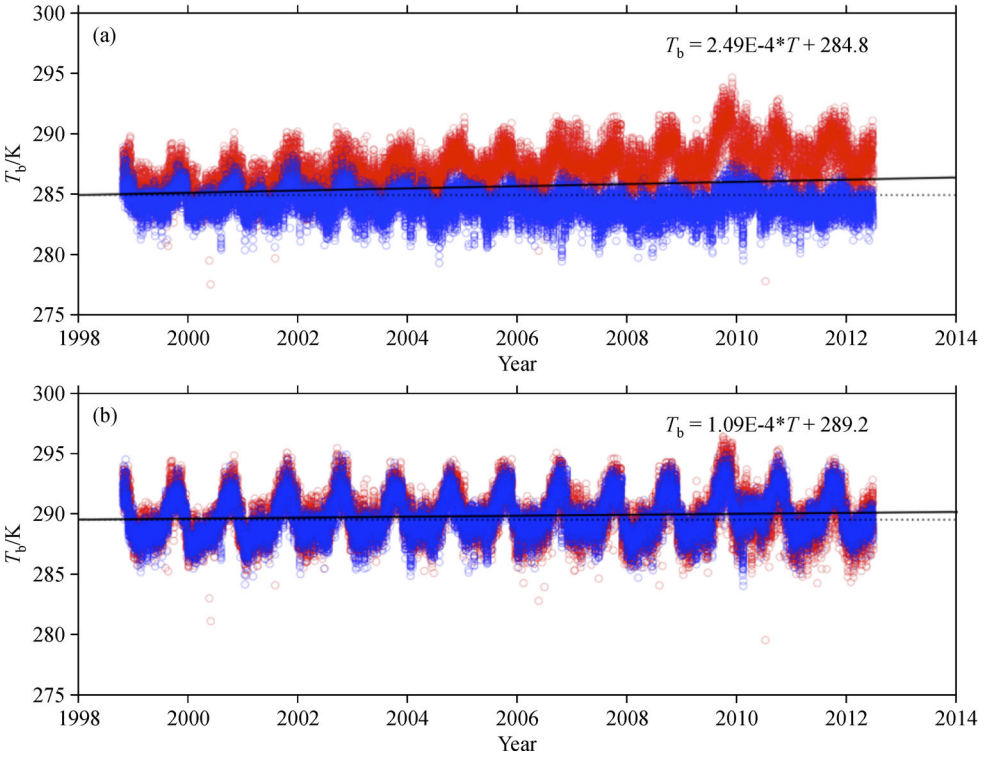

Fig. 6 Time series of brightness temperature observations of channel 1 from NOAA-15 at its ascending (red, nighttime, early morning) and descending (blue, daytime, later afternoon) nodes (a) without and (b) with a diurnal correction using 1200 LT as reference local time. The linear trend of brightness temperature observations is indicated by black line. Regression equations are added in the upper right corner, the unit of T is day.

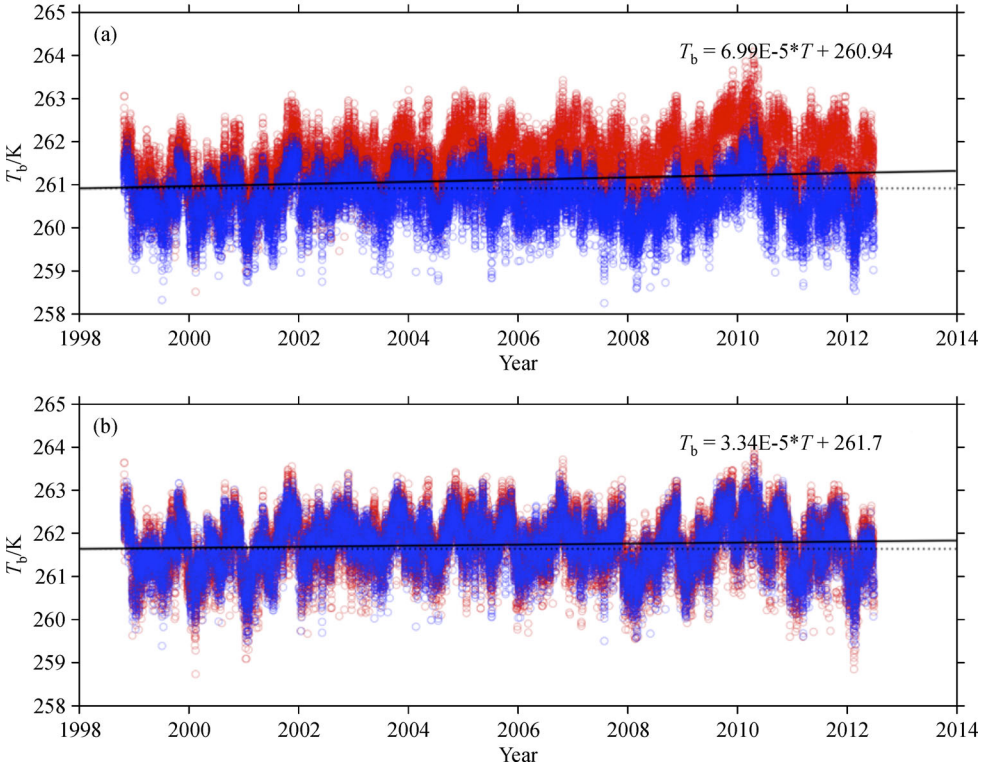

Fig. 7 Same as Fig. 6 except for channel 5.

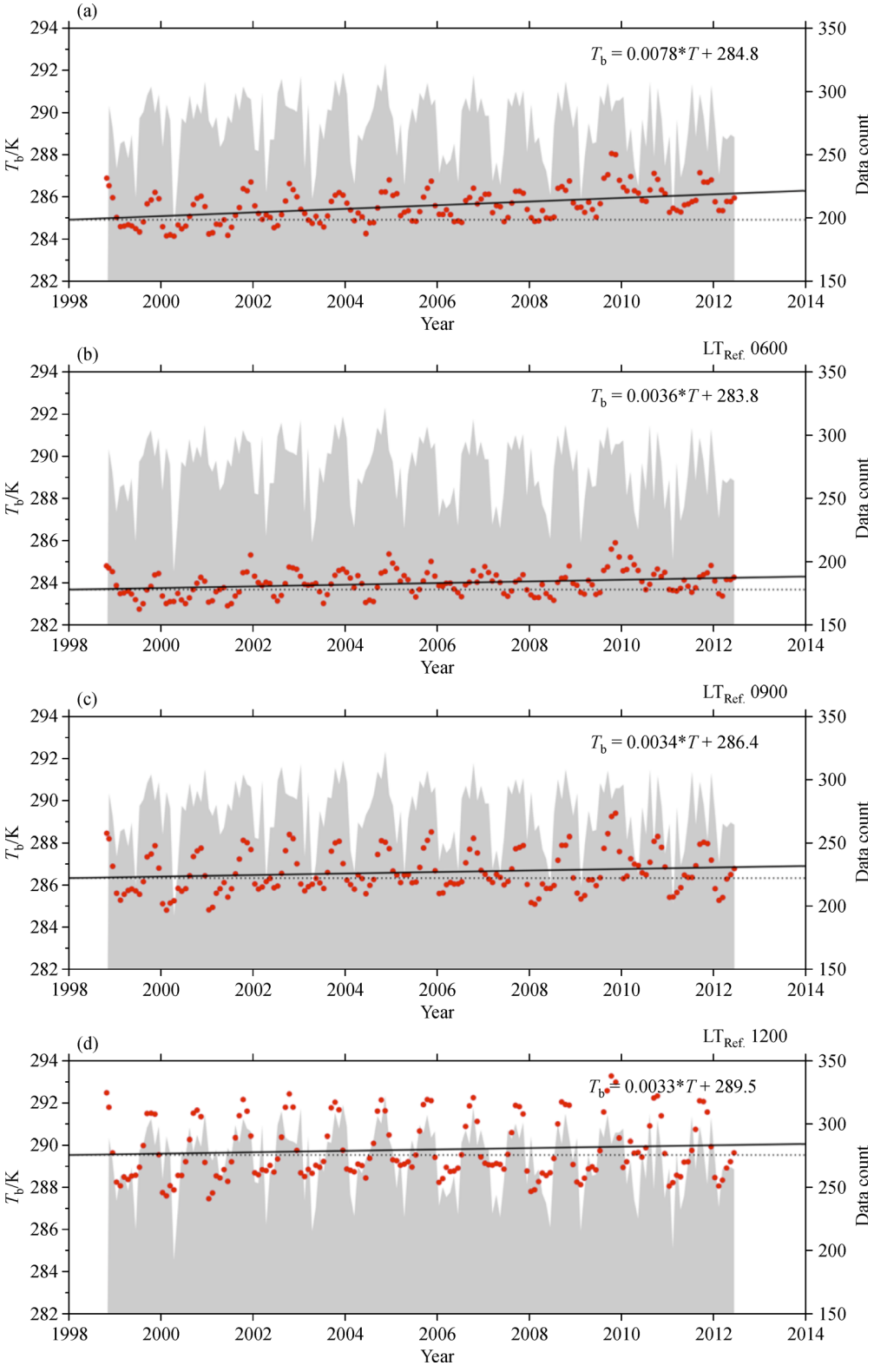

Fig. 8 Time series of monthly mean brightness temperature observations of NOAA-15 AMSU-A channel 1 (a) without and (b)−(d) with a diurnal correction using a reference local time at (b) 0600 LT, (c) 0900 LT or (d) 1200 LT. The linear trend of brightness temperature observations is indicated by a black line. The data counts are indicated in grey shading. Regression equations are added in the upper right corner, the unit of T is month.

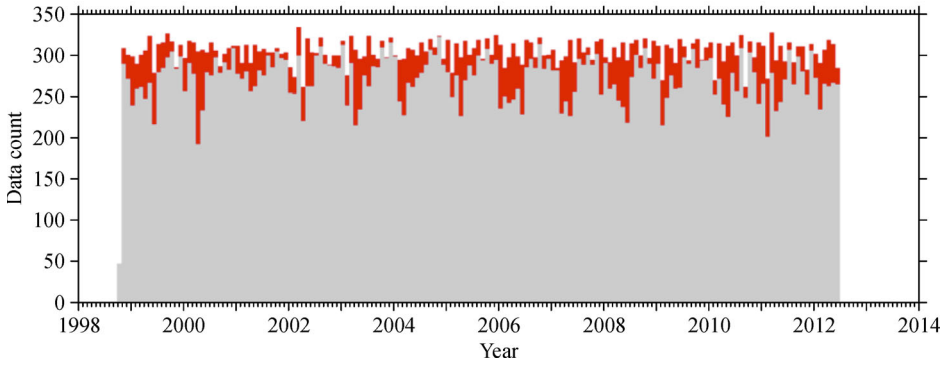

Fig. 9 Monthly data counts of NOAA-15 AMSU-A observations under the "no-rain" (grey) and "raining" (red) conditions over Amazon rainforest during the time period from October 1998 to June 2012.

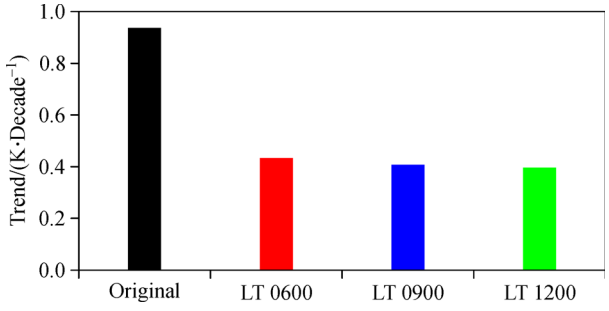

Fig. 10 Linear trends of brightness temperatures derived from monthly mean of NOAA-15 AMSU-A channel 1 before (black) and after applying diurnal correction with three different reference local times of 0600 LT (red), 0900 LT (blue), and 1200 LT (green).

a uniformly consistent annual variation is clearly seen. The trends of the data before and after diurnal correction also have large difference. It is thus concluded that the diurnal correction conducted in this study is quite effective. It shows that the warming trends of the diurnally corrected data are much smaller than those derived from the original data.

Decadal trends for all 15 AMSU-A channels derived from NOAA-15 only, and those derived from NOAA-15, -18, -19 and MetOp-A are shown in Figs. 12(a) and 12(b), respectively. The magnitudes of both the tropospheric warming trends (i.e., channels 1 – 8) and stratospheric (i.e., channels 9 – 11) cooling trends all decreased significantly after the inter-sensor calibration and diurnal correction. As mentioned before, the data from NOAA-15 AMSU-A channels 6, 11, and 14 are excluded from this study, and the data counts of these three channels are much fewer than other channels. Since the diurnal correction removes the diurnal signal induced by an orbital drift from the climate trend, the long-term temperature trends from satellite observations better reflect the warming of the physical temperature of the atmosphere.

6 Summary and conclusions

In this study, AMSU-A observations from NOAA-15, -18, -19, and MetOp-A during the time period from October 1998 to March 2013 are used for deriving a long-term temperature trend. The data from NOAA-15, -19, and MetOp-A are inter-calibrated with respect to those from NOAA-18 using the double difference method described in Section 2.2. The consistency of the AMSU-A stratospheric channel data from multiple satellites has been highly improved after applying an inter-sensor bias correction using the results calculated from a double difference method.

Once the inter-sensor biases are removed, a diurnal correction is applied to AMSU-A onboard the four POES satellites using near-nadir FOVs under "no-rain" conditions over the Amazon rainforest. The diurnal variations are well represented by the second order Fourier series for each channel in each month. It is found that the accuracy of the diurnal variation is improved by using the inter-calibrated data from multiple POES satellites. For data from NOAA-15, the diurnal correction effectively removes the orbital drift induced diurnal warming/cooling signal from the long-term trend for most of the channels. For the data from the four satellites, the diurnal correction also significantly improves the data consistency among the four POES satellites, especially for the window channels with relatively large diurnal variations. The diurnal correction also improves the decadal trends derived from multiple satellites data. After applying diurnal correction, the warming trends at different local times are approximately the same, but less than half of the trends derived from the data without applying the diurnal correction.

This study can be extended to other sensors such as the Microwave Sounding Unit (MSU) and Advanced Technology Microwave Sounder (ATMS) for obtaining satellite temperature sounding data over a longer time period. The same methodology can also be used for studies over other

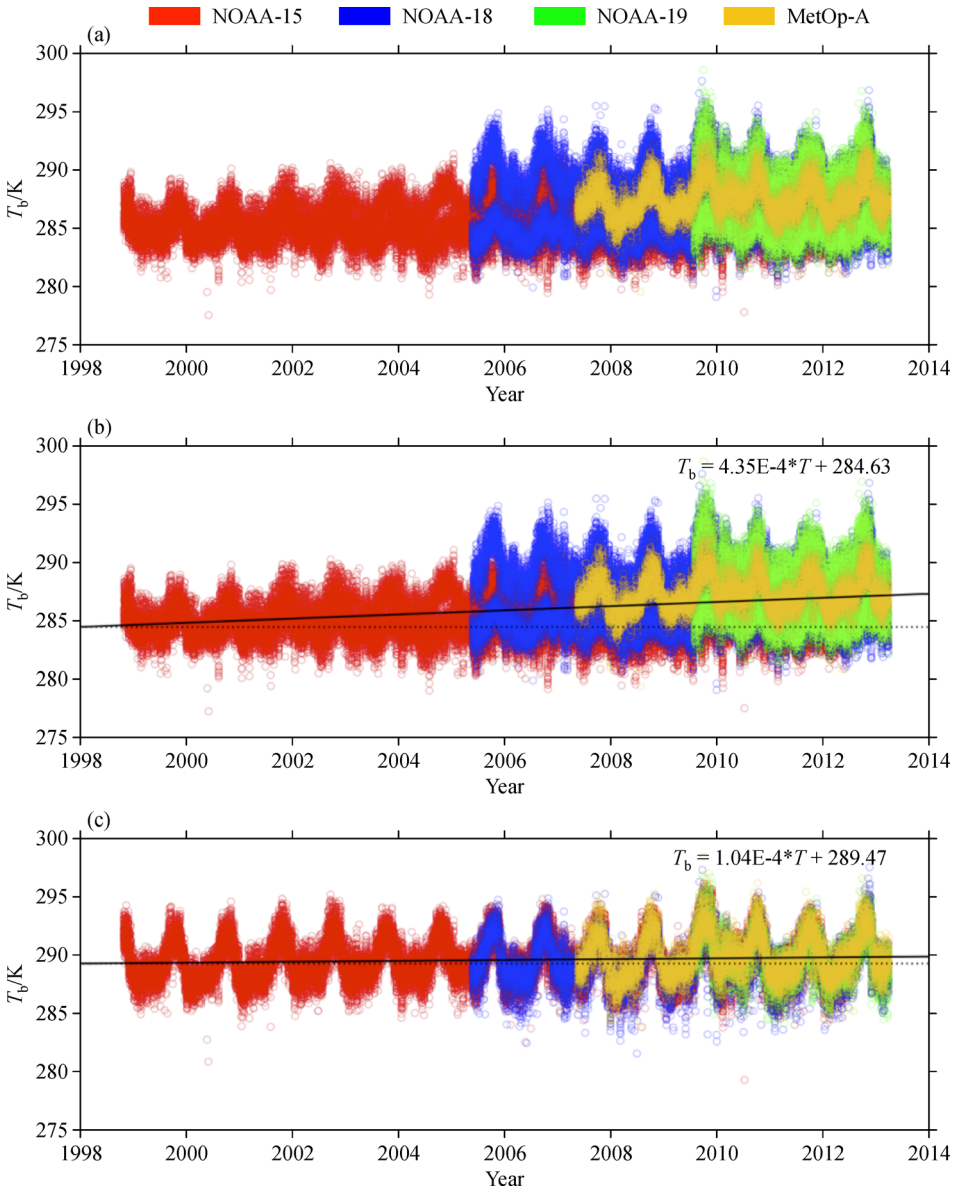

Fig. 11 Time series of channel 1 near-nadir observations from NOAA-19, NOAA-18, NOAA-15 and MetOp-A (a) without any inter-sensor bias correction nor diurnal correction and with (b) inter-sensor bias correction only (c) with both the inter-sensor bias correction and diurnal correction using a reference time at 1200 LT. The black solid line indicates the linear trend. Regression equations are added in the upper right corner, the unit of T is day.

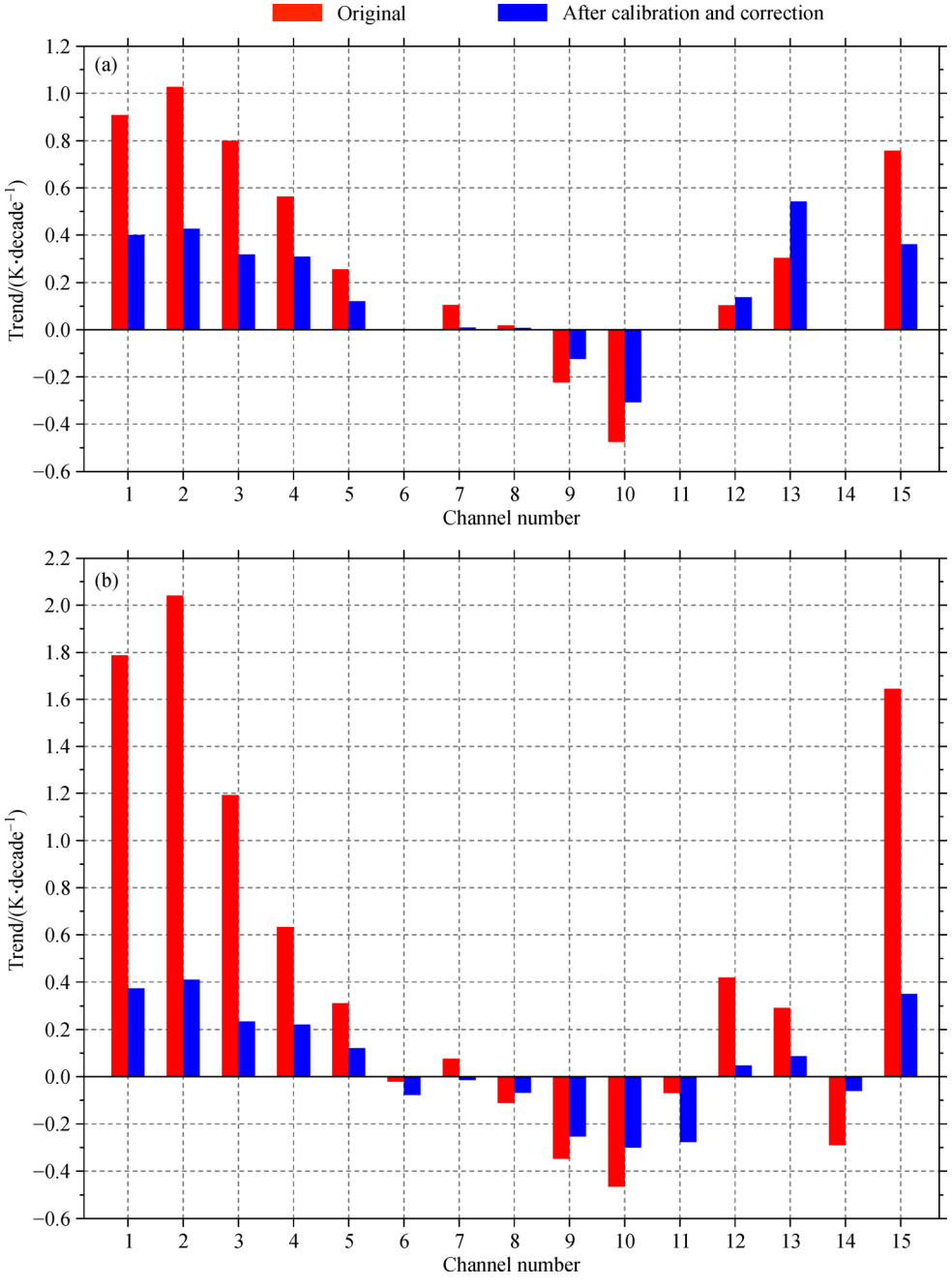

Fig. 12 Decadal linear trends of brightness temperature observations for all AMSU-A channels from (a) NOAA-15 only and (b) NOAA-15, -18, -19 and MetOp-A.

regions, especially the regions with large Diurnal Temperature Range (DTR) (e.g., Tibetan Plateau) but lack of conventional observations (e.g., Mid-Pacific Ocean).

Acknowledgements The work was supported by JPSS Proving Ground and Risk Reduction (PGRR) program (Project No. NA11OAR4320199), the National Natural Science Foundation of China (Grant No. 41505086) and National Oceanic and Atmospheric Administration (NOAA) under Grant NA14NES4320003.

References

Aldrich J (1998). Doing least squares: perspectives from Gauss and Yule. Int Stat Rev, 66(1): 61–81

Andersson E, Hollingsworth A, Kelly G, Lonnberg P, Pailleux J, Zhang Z (1991). Global observing system experiments on operational statistical retrievals of satellite sounding data. Mon Weather Rev, 119 (8): 1851–1864

Cao C, Weinreb M, Xu H (2004). Predicting simultaneous nadir overpasses among polar-orbiting meteorological satellites for the intersatellite calibration of radiometers. J Atmos Ocean Technol, 21 (4): 537–542

Clough S A, Shephard M W, Mlawer E J, Delamere J S, Iacono M, Cady-Pereira K E, Boukabara S, Brown P D (2005). Atmospheric radiative transfer modeling: a summary of the AER codes. J Quant Spectrosc Radiat Transf, 91(2): 233–244

Derber J C, Wu W S (1998). The use of TOVS cloud-cleared radiances in the NCEP SSI analysis system. Mon Weather Rev, 126(8): 2287–2299

Eyre J R, Kelly G A, McNally A P, Andersson E, Persson A (1993). Assimilation of TOVS radiance information through one-dimensional variational analysis. Q J R Meteorol Soc, 119(514): 1427–1463

Ferraro R R, Weng F, Grody N C, Zhao L (2000). Precipitation characteristics over land from the NOAA-15 AMSU sensor. Geophys Res Lett, 27(17): 2669–2672

Han Y, Weng F, Liu Q, van Delst P (2007). A fast radiative transfer model for SSMIS upper atmosphere sounding channels. Journal of Geophysical Research: Atmospheres, 112(D11): D11121

Kroodsma R A, McKague D S, Ruf C S (2012). Inter-calibration of microwave radiometers using the vicarious cold calibration double difference method. IEEE Journal of Selected Topics in Applied Earth Observations and Remote Sensing, 5: 1006–1013

Mears C A, Schabel M C, Wentz F J, Santer B D, Govindasamy B (2002). Correcting the MSU middle tropospheric temperature for diurnal drifts. Geoscience and Remote Sensing Symposium, 2002. IGARSS '02. 2002 IEEE International, 3: 1839–1841

Mo T (1996). Prelaunch calibration of the advanced microwave sounding unit-A for NOAA-K. IEEE Trans Microw Theory Tech, 44(8): 1460–1469

Mo T (2007). Diurnal variation of the AMSU-A brightness temperatures over the Amazon rainforest. IEEE Transactions on Geoscience and Remote Sensing, 45: 958–969

Privette J L, Fowler C, Wick G A, Baldwin D, Emery W J (1995). Effects of orbital drift on advanced very high resolution radiometer products: normalized difference vegetation index and sea surface temperature. Remote Sens Environ, 53(3): 164–171

Tian X, Zou X (2016). ATMS- and AMSU-A-derived hurricane warm core structures using a modified retrieval algorithm. J Geophys Res Atmos, 121(21): 12,630–12,646

Wang L, Goldberg M, Wu X, Cao C, Iacovazzi R A, Yu F, Li Y (2011). Consistency assessment of atmospheric infrared sounder and infrared atmospheric sounding interferometer radiances: double differences versus simultaneous nadir overpasses. Journal of Geophysical Research: Atmospheres, 116(D11): 755–764

Weng F (2007). Advances in radiative transfer modeling in support of satellite data assimilation. J Atmos Sci, 64(11): 3799–3807

Weng F, Grody N C (2000). Retrieval of ice cloud parameters using a microwave imaging radiometer. J Atmos Sci, 57(8): 1069–1081

Weng F, Zhao L, Ferraro R R, Poe G, Li X, Grody N C (2003). Advanced microwave sounding unit cloud and precipitation algorithms. Radio Sci, 38(4): 8068

Zou C, Goldberg M D, Cheng Z, Grody N C, Sullivan J T, Cao C, Tarpley D (2006). Recalibration of microwave sounding unit for climate studies using simultaneous nadir overpasses. Journal of Geophysical Research: Atmospheres, 111(D19): 5455–5464

Zou C, Wang W (2011). Intersatellite calibration of AMSU-A observations for weather and climate applications. Journal of Geophysical Research: Atmospheres, 116(D23): 23113

Zou X, Wang X, Weng F, Li G (2011). Assessments of Chinese Fengyun Microwave Temperature Sounder (MWTS) measurements for weather and climate applications. J Atmos Ocean Technol, 28(10): 1206–1227

Zou X, Weng F, Yang H (2014). Connecting the time series of microwave sounding observations from AMSU to ATMS for long-term monitoring of climate. Journal of Atmospheric & Oceanic Technology, 31(10): 2206–2222